Chemical Geology 493 (2018) 327–337

Contents lists available at ScienceDirect

Chemical Geology

journal homepage: www.elsevier.com/locate/chemgeo

Nitrogen abundance and isotope analysis of silicate glasses by secondary ionization mass spectrometry

Evelyn Füri[a,*], Etienne Deloule[a], Célia Dalou[a,b]

[a] Centre de Recherches Pétrographiques et Géochimiques, UMR 7358, CNRS-UL, 15 rue Notre Dame des Pauvres, BP20, 54501 Vandoeuvre-lès-Nancy Cedex, France
[b] University of Minnesota, Department of Earth Sciences, 108 Pillsbury Hall, Minneapolis, MN 55455, USA

ARTICLE INFO

Editor: K. Mezger

Keywords:
Nitrogen
SIMS
Reference material synthesis
Basaltic glass
Chondrules
Semarkona

ABSTRACT

Chondritic meteorites preserve extreme intra-sample $^{15}N/^{14}N$ variations, which exceed, in some cases, the range of nitrogen isotope ratios observed at the Solar System scale. These observations are based on in situ analyses of CN^- molecular ions by secondary ionization mass spectrometry (SIMS) in carbon-rich phases. The distribution of nitrogen and its isotopes in silicate minerals and glasses has not been investigated to this date due to the lack of an appropriate analytical protocol, as well as of suitable N-bearing standards. In order to improve our knowledge of the nitrogen signature of both extraterrestrial and terrestrial silicate samples, we have developed a protocol for determining precise and accurate nitrogen abundances (and isotope ratios) in basaltic glasses using high mass resolution SIMS. Twelve (C-)N-bearing synthetic basaltic glasses, containing between < 1 and 18,443 ± 966 ppm N, form the suite of reference materials for this study. By targeting the CN^-, NO^-, AlN^-, and SiN^- secondary molecular ions, nitrogen abundances can be detected down to the ppm level in both carbon-bearing and carbon-free glasses. The analytical precision and reproducibility of isotope ratios in the form of $^{15}N^{16}O^-/^{14}N^{16}O^-$ is on the order of 11‰ and 10 to 17‰ (2σ), respectively, for reference glasses containing ≥100 ppm N. Thus, nitrogen isotope ratios can be determined with an uncertainty that is small enough to resolve nitrogen isotope variations in extraterrestrial silicates. The study of four chondrules of the ordinary chondrite Semarkona (LL3.0) reveals that the nitrogen distribution in the mesostasis is highly heterogeneous, with concentrations ranging from 0 to 1099 ± 168 ppm. The $\delta^{15}N$ values in mesostasis, olivine, and pyroxene vary between −36 ± 50‰ and +55 ± 72‰, indicating that silicate phases in chondrules do not host particularly ^{15}N-poor nitrogen.

1. Introduction

Nitrogen isotopes provide a powerful tool for tracing the origin of volatile elements on planetary bodies because the relative proportion of ^{14}N and ^{15}N shows outstanding variability among different Solar System objects and reservoirs (Füri and Marty, 2015). Although turbulent mixing regionally homogenized the material available for planet formation – resulting in similar nitrogen isotope compositions for Earth and the Moon, the interior of Mars, and most chondrite groups ($\delta^{15}N \approx 0 \pm 50$‰; e.g., Füri et al., 2015a; Kerridge, 1985; Kung and Clayton, 1978; Mathew and Marti, 2001; Pearson et al., 2006) –, micron-sized zones with extreme nitrogen isotopic anomalies remain preserved in some chondritic meteorites. So-called ^{15}N-hotspots have been detected in the insoluble organic matter of carbonaceous chondrites ($\delta^{15}N = 3200 \pm 700$‰; Busemann et al., 2006) and in lithic clasts of the Isheyevo meteorite ($\delta^{15}N = 4200 \pm 1500$‰ to 4900 ± 300‰; Bonal et al., 2010; Briani et al., 2009). In contrast, osbornite (TiN) within a calcium-aluminum-rich inclusion of Isheyevo records an exceptionally ^{15}N-poor, solar-like nitrogen isotope signature ($\delta^{15}N = -364 \pm 12$‰; Meibom et al., 2007). Bulk chondrules, millimeter-sized silicate spheres in chondrites, also display a significant range of $^{15}N/^{14}N$ ratios ($\delta^{15}N \approx -100$ to +170‰; Das and Murty, 2009; Fredriksson et al., 1985; Kung and Clayton, 1978; Mahajan and Murty, 2003; Murty and Marti, 1985) which lead previous authors to suggest that chondrule precursors carried various nitrogen components with distinct isotopic compositions, and that this heterogeneity was preserved during the high-temperature chondrule forming process(es). Silicates are inferred to be the carriers of isotopically light nitrogen in chondrules, whereas organics and metals or metal sulfides are thought to represent the ^{15}N-enriched endmember (Fredriksson et al., 1985; Murty and Marti, 1985). However, previous data were obtained through bulk analyses, and the nitrogen isotopic signature of distinct chondrule phases (mesostasis, silicate minerals, melt inclusions, metals, sulfides) has not been investigated to this date. Since chondrules have

* Corresponding author.
E-mail address: efueri@crpg.cnrs-nancy.fr (E. Füri).

https://doi.org/10.1016/j.chemgeo.2018.06.008
Received 9 January 2018; Received in revised form 9 June 2018; Accepted 12 June 2018
Available online 21 June 2018

recently been shown to contain relict olivine grains inherited from chondrule precursors (Marrocchi et al., 2018), and to preserve significant hydrogen and oxygen isotopic heterogeneities (Deloule and Robert, 1995; Marrocchi et al., 2016, 2018), in situ analyses are crucial for better understanding the origin and distribution of nitrogen in chondrules.

Nitrogen abundances and isotope ratios of geologic samples have historically been analyzed using isotope ratio mass spectrometers operated in dynamic pumping mode or noble gas mass spectrometers operated under static vacuum conditions (e.g., Frick and Pepin, 1981; Hashizume and Marty, 2004; Javoy and Pineau, 1991; Thiemens and Clayton, 1983). Although the latter technique requires only a small amount of material (≤5 mg; e.g., Füri et al., 2015a), these bulk analytical methods are destructive and do not provide any information on the spatial distribution of nitrogen within the sample. Nuclear reaction (Mosbah et al., 1993; Varela et al., 2003) and electron microprobe analyses (EPMA; Kadik et al., 2011; Li et al., 2015; Roskosz et al., 2013; von der Handt and Dalou, 2016) allow for in situ measurements of nitrogen abundances in silicate glasses with detection limits on the order of 10 and 100 s–1000 s ppm, respectively. Since nitrogen nuclear microanalysis is based on the $^{14}N(d,p)^{15}N$ reaction, and EPMA cannot distinguish between isotopes of the same element, isotope ratio measurements are not feasible by these techniques.

Secondary ionization mass spectrometry (SIMS) analysis represents a quasi non-destructive method for determining chemical and isotopic variations with a high lateral resolution (at a scale as small as ≤10 μm) or a high depth resolution (≤10 nm). The measurement of nitrogen by SIMS is challenging because it does not form a stable elemental negative ion. However, an intense CN^- signal forms in the presence of carbon, when the sample surface is bombarded with a Cs^+ ion beam (Zinner et al., 1989). Thus, nitrogen isotope ratios have successfully been determined in the form of $^{12}C^{15}N^-/^{12}C^{14}N^-$ in a range of carbon-rich materials such as pollen (e.g., Lhuissier et al., 2000), organic matter (e.g., Aléon et al., 2003; Busemann et al., 2006; Thomen et al., 2014), graphite (e.g., Mostefaoui et al., 2005), diamond (e.g., Hauri et al., 2002), SiC (Marty et al., 2011; Zinner et al., 1989), osbornite (Meibom et al., 2007), and iron meteorites (e.g., Sugiura, 1998). As an alternative, for carbon-free samples such as silicate minerals and glasses, the NO^- signal can be targeted for nitrogen abundance measurements, as demonstrated by Li et al. (2013) and Regier et al. (2016). The lack of an appropriate analytical protocol, as well as of suitable N-bearing standards, has so far prevented the use of SIMS for nitrogen isotope analyses of silicates.

Here we present a novel protocol for in situ nitrogen abundance and isotope analyses in basaltic silicate glasses. The CAMECA IMS 1280 HR2 at the Centre de Recherches Pétrographiques et Géochimiques (CRPG, Nancy) can achieve a high mass resolution, i.e., MRP = m/Δm up to 18,000 in this study, allowing significant isobaric interferences from neighboring masses on the CN^-, NO^-, AlN^-, and SiN^- signals to be resolved. By targeting these secondary molecular ions, nitrogen abundances can be detected down to the ppm level in both carbon-bearing and carbon-free silicate samples. Furthermore, isotope ratios in the form of $^{15}NO^-/^{14}NO^-$ can be determined with an uncertainty of < 20‰ for reference glasses containing ≥100 ppm nitrogen. Hence, this technique is key for the study of nitrogen trapped within micron-sized silicate phases such as chondrule components (e.g., mesostasis).

2. Reference materials used for nitrogen analyses by SIMS

2.1. N-bearing basaltic glasses synthesized at atmospheric pressure

To investigate the nitrogen solubility in tholeiitic melt, Humbert (1998) experimentally produced basaltic glass samples with a range of nitrogen concentrations (< 1 to ≥5000 ppm). Nitrogen equilibration experiments were carried out for 36 to 48 h at a temperature of 1400 to 1425 °C and at atmospheric pressure in a GERO HTVR 70–250 vertical drop-quench furnace over a range of 18 log units of oxygen fugacity in a C-N-O vapor system (see Libourel et al. (2003) for details). Subsequently, the nitrogen content and isotopic composition of the quenched run products was determined by CO_2 laser extraction static mass spectrometry (Humbert et al., 2000). The solubility of nitrogen in basaltic melt was found to be highly sensitive to the oxygen fugacity, with a drastic increase of the nitrogen concentration by several orders of magnitude under reducing conditions (i.e., between logfO_2–10.7 and −18). Libourel et al. (2003) proposed that this solubility increase can be related to changes in the mechanism of nitrogen dissolution in silicate melt: under oxidizing conditions, nitrogen dissolves physically as a N_2 molecule, whereas under reducing conditions, nitrogen is chemically bounded to the silicate melt network as N^{3-} species. Thus, basaltic glasses covering a wide range of nitrogen contents were obtained by simply varying the redox conditions of the equilibration experiments. Eight nitrogen-bearing glasses synthesized by Humbert (1998) are used in this study as reference materials for nitrogen abundance and isotope analyses by SIMS (Table 1). These glasses cover a concentration range between < 1 and 3906 ± 188 ppm N, and their $\delta^{15}N$ value (where $\delta^{15}N$ is the permil deviation from the atmospheric $^{15}N/^{14}N$ ratio of 0.003676) has been shown to be close to −4 ± 1‰ (Humbert, 1998), which corresponds to the isotopic composition of the N_2 gas used for the experiments.

2.2. C-N-bearing basaltic glasses synthesized at high pressure

Six C-N-rich glasses were synthesized from N-MORB-like (Presnall and Hoover, 1984) starting material, obtained by mixing pre-dried, spectroscopically pure oxides and carbonates. The starting composition was prepared Fe-free to prevent iron nitride crystallization. The mixture was decarbonated by heating, ground in ethanol in an agate mortar, and nitrogen was added by using between 0.3 and 5 wt% Si_3N_4, which has a strong reducing effect. Although in the absence of Fe, the fO_2 could not be measured, it is expected that the samples are reduced within the same range as those of Dalou et al. (2016), i.e., −13 < log fO_2 < −8.5.

Nitrogen equilibration experiments were carried out for six hours in a ½-inch piston cylinder at 1.2 ± 0.1 GPa and 1400 °C at the University of Minnesota. From outside to inside, assemblies consisted of a CaF_2 sleeve surrounding a graphite furnace, and MgO cell parts, which were dried beforehand at 1000 °C for 4 h and stored in a drying oven at 110 °C. The starting material was loaded into a graphite capsule to prevent nitrogen diffusion into metal capsules, to ensure reducing conditions (thus promoting the nitrogen dissolution into the melt phase; e.g., Kadik et al., 2015; Libourel et al., 2003), and to provide a source of carbon. The graphite capsule was placed into an MgO sleeve and isolated from the thermocouple by a 1 mm MgO ring. The temperature was measured with a type B ($Pt_{70}Rh_{30}/Pt_{94}Rh_6$) thermocouple to within ± 2 °C of the set point (Zhang and Hirschmann, 2016). Experiments were temperature-quenched rapidly before decompression (at a rate of ~175 °C/s) by turning off the power to the furnace. The recovered capsules were cut lengthwise using a wire saw, and one half of each experimental charge was roughly ground into sub-millimetric fragments.

The clearest glass fragments (free of visible graphite, as observed under the microscope) are used as SIMS calibrants for this study, and a few chips of each sample were targeted for nitrogen concentration and isotope ratio analyses by CO_2 laser extraction static mass spectrometry (Appendix A). Total nitrogen abundances of the six glasses vary between 383 ± 33 and 18,443 ± 966 ppm, with $\delta^{15}N$ values of −9.9 to −0.7‰ (± 2.5‰) (Table 1 and Appendix A), and represent both N_2 and N-H species (Dalou et al., 2017). Complementary SIMS analyses revealed that the CO_2-equivalent carbon content of the glasses is highly variable and heterogeneous, likely due to the presence of micron-sized graphite inclusions (Table 1 and Appendix B). Furthermore, the glasses contain between 0.8 and 2.4 wt% H_2O, which is assumed to have been

Table 1
Nitrogen[a], water, and carbon content[b], as well as major element composition[c], of the reference materials used for SIMS analyses.

Calibrant ID	N (ppm)	H_2O (wt%)	CO_2 (ppm)	SiO_2 (wt%)	Al_2O_3 (wt%)	MgO (wt%)	CaO (wt%)	Na_2O (wt%)	TiO_2 (wt%)
Glasses synthesized at atmospheric pressure									
CM-1#13	0.022 ± 0.034	b.d.	b.d.	56.5(4)	17.0(2)	9.0(2)	12.7(3)	2.7(1)	1.9(1)
CM-1#10	1.4 ± 0.5	b.d.	b.d.	56.9(4)	17.5(2)	9.4(2)	13.4(2)	1.8(1)	0.9(2)
CM-1#3H	1.7 ± 0.3	b.d.	b.d.	46.3(3)	22.4(2)	12.7(2)	18.6(3)	0.1(1)	b.d.
CM-1#9	136 ± 7	b.d.	b.d.	57.0(4)	17.7(2)	9.3(1)	13.5(2)	0.3(1)	1.9(1)
CB-2#3A	162 ± 8	b.d.	b.d.	44.0(2)	18.0(2)	11.0(2)	25.8(3)	b.d	1.5(1)
CM-1#4A	1334 ± 118	b.d.	b.d.	58.3(3)	16.5(2)	8.9(2)	13.8(3)	b.d.	1.5(1)
CM-1#1H	1511 ± 149	b.d.	b.d.	56.7(4)	18.3(2)	9.5(1)	13.9(3)	0.1(1)	1.8(1)
CB-2#1	3906 ± 188	b.d.	122	42.9(4)	19.5(2)	10.2(2)	27.7(3)	b.d.	0.2(1)
Glasses synthesized at high pressure									
704	383 ± 33	1.9	241	51.8(3)	17.2(3)	10.8(1)	13.5(2)	2.2(1)	0.9(1)
703	714 ± 64	1.4	≥105	52.2(3)	17.7(1)	10.8(2)	13.7(1)	2.3(1)	1.0(1)
702	2228 ± 286	0.8	391	54.0(4)	17.3(2)	10.7(2)	13.4(1)	2.3(1)	1.0(1)
701	3284 ± 233	0.8	≥438	53.7(3)	17.6(2)	10.8(1)	13.5(2)	2.3(1)	1.0(1)
710	6883 ± 419	0.8	565	54.9(4)	16.4(3)	11.1(6)	13.7(4)	2.1(1)	0.9(1)
711	18,443 ± 966	0.9	≥916	58.2(4)	16.2(3)	10.1(2)	12.6(2)	2.1(1)	0.5(5)
Other calibrants									
SiC	~10 ppm								

[a] The nitrogen content of the glasses was determined by CO_2 laser extraction static mass spectrometry at the CRPG noble gas facility (Humbert, 1998; Humbert et al., 2000; Appendix A).

[b] The H_2O and CO_2 content of the glasses was determined using the CAMECA 1280 HR2 ion microprobe at the CRPG (see Appendix B for details). b.d.: below detection limit.

[c] The major element composition of the glasses was determined using the Cameca SX-100 electron microprobe at the Université de Lorraine (Service Commun de Microscopies Electroniques et de Microanalyses X). Uncertainties (1σSD) given in parentheses refer to the last digit.

introduced into the samples as a result of air contamination of the starting material and/or the high-pressure assembly parts.

2.3. N-bearing SiC

A fragment of silicon carbide (SiC) containing terrestrial nitrogen was used in a previous study as a calibrant for SIMS analysis of solar wind nitrogen implanted into the SiC quadrant of the Solar Wind Concentrator on board NASA's Genesis spacecraft (Marty et al., 2011). The concentration of nitrogen in this material is ~10 ppm, and its $^{15}N/^{14}N$ ratio was found to be $3.722 \times 10^{-3} \pm 1.29 \times 10^{-5}$ ($\delta^{15}N = 12.5 \pm 3.5‰$) by laser ablation static mass spectrometry analysis (Marty et al., 2011). Given the high purity of the SiC fragment, it is ideal for identifying the peaks of interest when measuring nitrogen in the form of CN^- or SiN^-. However, the peculiar composition of this material rules out its use as a calibrant for nitrogen concentration and isotope ratio analyses of silicates, as standards must be close in composition to the samples in order to minimize matrix effects.

3. Analytical protocol for nitrogen analyses by SIMS

The CAMECA 1280 HR2 ion microprobe at the CRPG was used for in situ nitrogen abundance and isotope analyses. Polished fragments of the different glasses and the SiC calibrant were mounted in high-purity indium and coated with gold. Prior to each analytical session, the sample mounts were left in the airlock of the instruments for at least 48 h in order to ensure thorough removal of any terrestrial adsorbed water before introduction into the sample chamber. In addition, a liquid nitrogen cold trap allowed maintaining a pressure of $\leq 5 \times 10^{-9}$ Torr during analyses. This is critical for minimizing hydride species formation.

Spot analyses of negatively charged molecular nitrogen ions at different mass stations were carried out using a 10 keV Cs^+ primary ion beam with a current of ~10 nA and a normal-incidence electron gun for charge compensation. Spot sizes were on the order of 20 μm in diameter. The samples were pre-sputtered for 180 s with a beam rastering of 10 × 10 μm prior to signal acquisition in order to minimize surface contamination. For abundance and isotope ratio analyses, the beam was rastered by 5 × 5 μm, and a dynamical transfer operating system was used to compensate the primary rastering by recentering the beam in the secondary optic of the ion probe. Before starting the data acquisition, the secondary ion beam was automatically centered in *x* and *y* on the field aperture and the contrast aperture, followed by a mass centering routine in order to compensate for any magnetic field drift.

3.1. Nitrogen analysis in the form of CN^- at masses 26 and 27

For the C-N-rich glasses and the SiC calibrant, the $^{12}C^{14}N^-$ and $^{12}C^{15}N^-$ ion signals were acquired on an electron multiplier with a mass resolution of 11,000 at 10% of the peak height. High-resolution mass spectra obtained for the SiC calibrant allow clearly identifying the peaks of interest because signals from neighboring masses such as $^{25,26}MgH$ and $^{10,11}BO$ are absent. Fig. 1 shows that $^{12}C^{14}N^-$ is completely separated from $^{13}C_2^-$ and $^{10}BO^-$, as is $^{12}C^{15}N^-$ from $^{11}BO^-$ and $^{13}C^{14}N^-$. For nitrogen abundance measurements, the $^{12}C^{14}N^-$ molecular ion was analyzed with a count time of 6 s for 30 cycles (Supplementary Table S1). The $^{12}C^-$ (4 s) and $^{30}Si^-$ (4 s) count rates were acquired on a Faraday cup in peak-jumping mono-collection mode during each cycle in order to monitor the carbon distribution in the samples and the stability of secondary ion intensities, respectively. The secondary ion intensity ratio $^{12}C^{14}N^-/^{30}Si^-$ shows an excellent correlation ($R^2 = 0.99$) with the known nitrogen contents, even though the count rates for $^{12}C^-$ in glasses 701, 703, and 711 were found to vary significantly with depth over the course of a 30-cycle analysis (Fig. 2), as well as between different spots. The variation of the $^{12}C^-$ signal is likely due to the presence of nano- or micrometer-sized graphite inclusions, clustered in some parts of the glasses, as observed by scanning electron microscope imaging. Notably, these inclusions have a limited effect on the intensity of the $^{12}C^{14}N^-$ signal, as illustrated, for example, by measurement cycles #3 to #8 of the N-richest glass 711 (Fig. 2b). This indicates that the graphitic inclusions do not contain a significant amount of nitrogen.

With this instrument configuration, an average $^{12}C^{14}N^-$ ion yield of 1.3 cps/ppmN/nA is obtained for the silicate glasses. This would be sufficient for precise nitrogen abundance analyses of the synthetic glasses that contain hundreds to thousands of ppm nitrogen; however,

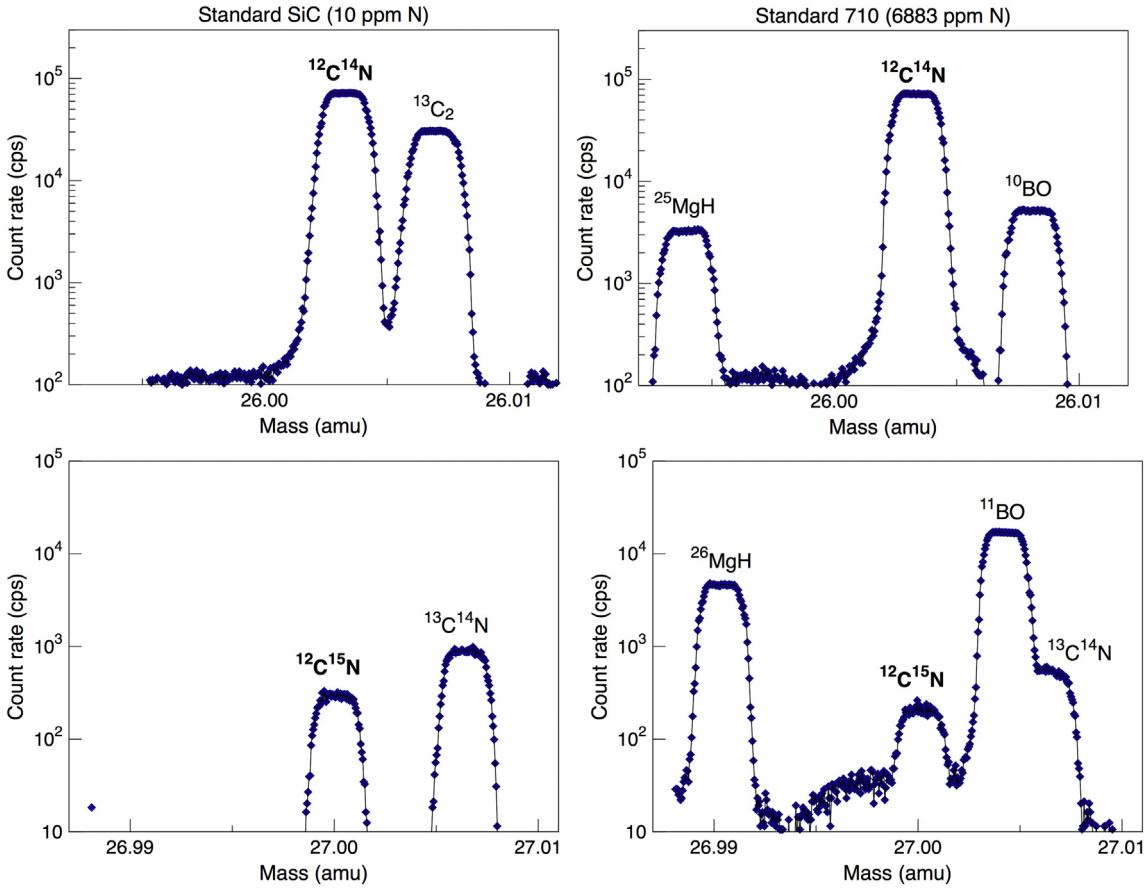

Fig. 1. High-resolution mass spectra at mass stations 26 and 27 for the silicon carbide (SiC) calibrant (left) and the 710 glass (right). Data were acquired with a mass resolution (m/Δm) of ~11,000.

repeat analyses of each calibrant yield $^{12}C^{14}N^-/^{30}Si^-$ ratios that are reproducible only within 4 to 7% (1σSD). This is consistent with the variations observed during the nitrogen concentration measurements by CO_2 laser extraction static mass spectrometry (Table 1 and Appendix A), and possibly reflects a significant degree of heterogeneity in the nitrogen content of the experimental run products. Given the important C-N heterogeneities in the glasses, precise isotope ratios could not be obtained. In contrast, repeat $^{12}C^{14}N^-$ (6 s) and $^{12}C^{15}N^-$ (12 s) analyses (n = 13) of the SiC calibrant yield an average $^{12}C^{15}N^-/^{12}C^{14}N^-$ ratio of $3.634 \times 10^{-3} \pm 1.13 \times 10^{-5}$ ($\delta^{15}N = -11.3 \pm 3.1‰$, 2σ), indicating that the analytical precision of SIMS and static mass spectrometry analysis is comparable for this sample. The instrumental mass fractionation ($\Delta_{inst} = -23.8 \pm 6.6‰$) observed here for SiC is consistent with that reported by Marty et al. (2011), i.e., $\Delta_{inst} = -29.7 \pm 8.3‰$ and $-25.6 \pm 11.6‰$.

Overall, the results obtained here demonstrate that natural C-N-bearing silicate samples can be targeted for nitrogen analyses in the form of CN^- by SIMS. Regier et al. (2016) pointed out that the $^{12}C^{14}N^-$ ion yield likely depends on the limiting element, i.e., a low carbon concentration may limit the efficiency of C-N recombination reactions.

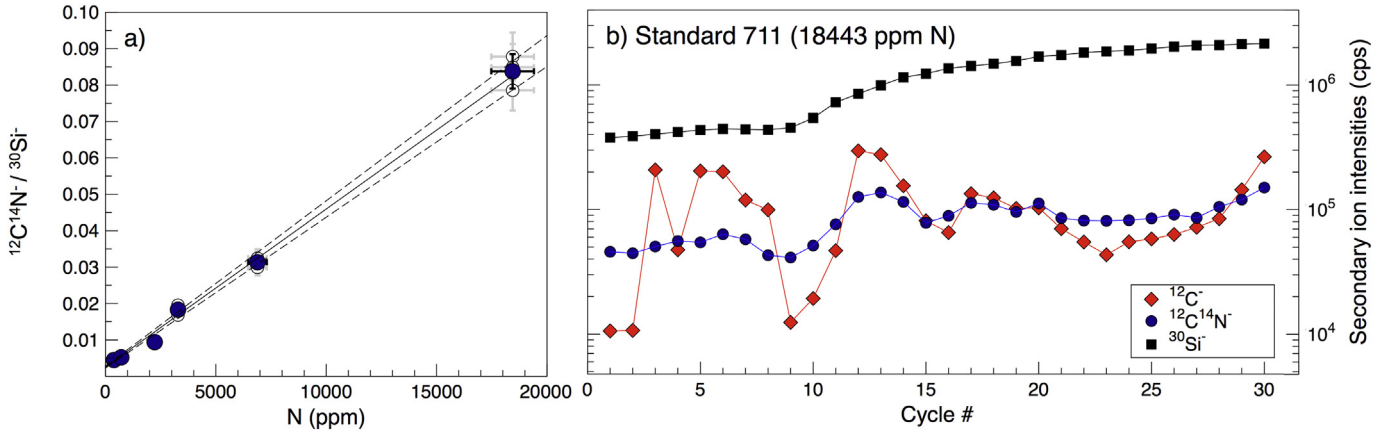

Fig. 2. a) Relationship between the secondary ion intensity ratio $^{12}C^{14}N^-/^{30}Si^-$ and the known nitrogen content of the six C-N-rich glasses (open symbols: individual analyses; filled symbols: average for each calibrant). The data were regressed using IsoplotR (Vermeesch, 2018). b) Evolution of the secondary ion intensities $^{12}C^-$, $^{12}C^{14}N^-$, and $^{30}Si^-$ during a 30-cycle measurement of the N-richest glass 711.

They therefore emphasized that the carbon content of unknowns should be comparable of that of the standards used for calibration. However, the $^{12}C^{14}N^-$ ion yield shows little variation among the glasses analyzed here, and the $^{12}C^{14}N^-/^{30}Si^-$ ratio shows a linear relationship with the known nitrogen abundance, despite the highly variable carbon content. Thus, the carbon heterogeneities do not appear to significantly affect the efficiency of C-N recombination reactions that occur at or near the sample surface during sputtering. Only the SiC calibrant (containing ~10 ppm nitrogen) stands out in that its $^{12}C^{14}N^-$ ion yield is > 1000 cps/ppmN/nA (Fig. 1) which can likely be attributed to a significant matrix effect given the peculiar composition of this material.

3.2. Nitrogen analysis in the form of NO^- at masses 30 and 31

With the exception of the SiC fragment, all glasses listed in Table 1 can be used as reference materials for nitrogen analyses in the form of NO^-. For this approach, a mass resolution of 5550 would be sufficient to determine nitrogen abundances (i.e., to resolve the $^{14}N^{16}O^-$ peak from the neighboring $^{28}SiH_2^-$ peak). However, isotope ratio measurements require a mass resolution of ≥10,725 in order to separate the $^{15}N^{16}O^-$ peak from $^{29}SiH_2^-$. This is of particular importance for water-rich samples, such as the glasses synthesized at high pressure (Table 1); as shown in Fig. 3, the peak intensities of the silicon hydrides are several orders of magnitude higher for glass 701, with a water content of 0.8%, than for glass CB-2#1, with a water content below detection limit.

In order to establish the relationship between the $^{14}N^{16}O^-$ ion count rate and the known nitrogen concentration of the glasses, the $^{14}N^{16}O^-$ ion intensity was measured by ion counting on an electron multiplier, together with the $^{30}Si^-$ and $^{16}O_2^-$ signals measured on a Faraday cup, in peak jumping mode (m/Δm = 11,000 at 10% of the peak height). Twenty-five cycles were collected for each analysis through the mass sequence $^{27}Al^-$ (4 s), $^{30}Si^-$ (4 s), $^{14}N^{16}O^-$ (6 s), $^{15}N^{16}O^-$ (20s), $^{16}O_2^-$ (4 s) (Supplementary Table S2). The $^{30}Si^-$ signal increased significantly, i.e., by a factor of three to four, during all analyses, indicating that the $^{30}Si^-$ emissivity is enhanced by Cs^+ implantation and build-up (Thomen et al., 2014, and references therein). In contrast, the $^{16}O_2^-$ count rates remained constant, implying that the O-O recombination reaction rates are not affected by surface implantation of Cs^+. It is also noteworthy that the ratio between the secondary molecular ions N-O and O-O is close to the atomic N/O ratio of the glasses analyzed here (Fig. 4a). This implies that their overall yields – after sputtering, extraction, and recombination – are comparable, yet likely depend on the sample matrix (e.g., degree of polymerization) and the nitrogen speciation. Therefore, the best correlation with the known nitrogen content is obtained when the $^{14}N^{16}O^-$ count rate is normalized by the $^{16}O_2^-$ signal (Fig. 4b). For these analytical conditions, the reproducibility of the secondary ion intensity ratio $^{14}N^{16}O^-/^{16}O_2^-$ was ≤4% (2σSD) for the glasses containing ≥162 ppm N. This uncertainty is comparable to, yet slightly smaller than, that of nitrogen concentration measurements by CO_2 laser extraction static mass spectrometry (Appendix A).

The $^{14}N^{16}O^-$ signal obtained for the nitrogen-poorest glass CM-1#13 (0.022 ± 0.034 ppm N) was only 2.9 ± 0.9 cps, indicating the nitrogen background – and any tailing from neighboring hydride species – is negligible for this analytical configuration. The average $^{14}N^{16}O^-$ ion yield, observed for the twelve glasses with nitrogen concentrations ≤3906 ppm, is 2.1 cps/ppmN/nA. The two glasses that contain the largest amount of water (i.e., 1.9 wt% H_2O in 704 and 1.4 wt% H_2O in 703; Table 1) show significantly higher $^{14}N^{16}O^-$ ion yields of 3.0 cps/ppmN/nA, and, as a result, they plot above the calibration line shown in Fig. 4b. Regier et al. (2016) observed the opposite effect; higher water contents resulted in lower NO^- signals for basaltic glasses. However, the variable ion yields observed here may also be

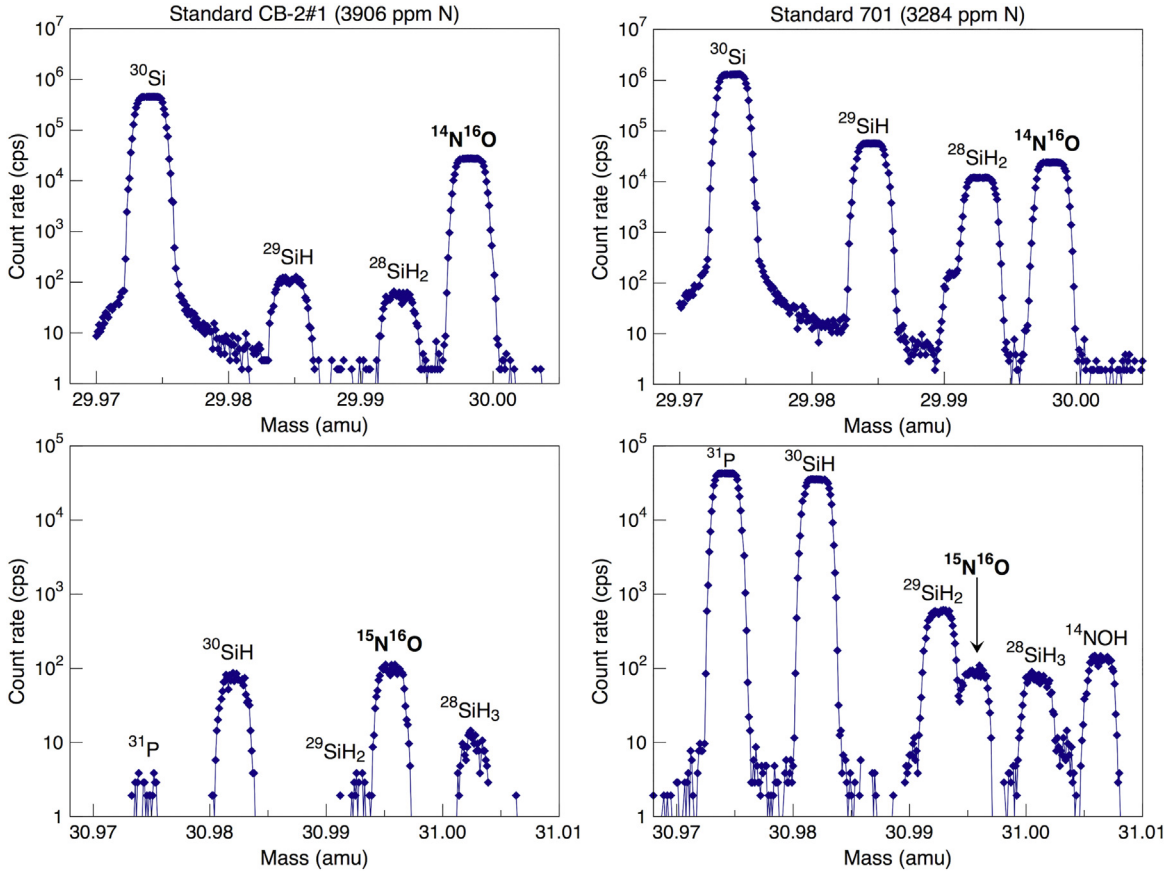

Fig. 3. High-resolution mass spectra at mass stations 30 and 31 for glasses CB-2#1 (left) and 701 (right) obtained with a mass resolution (m/Δm) of ~11,000.

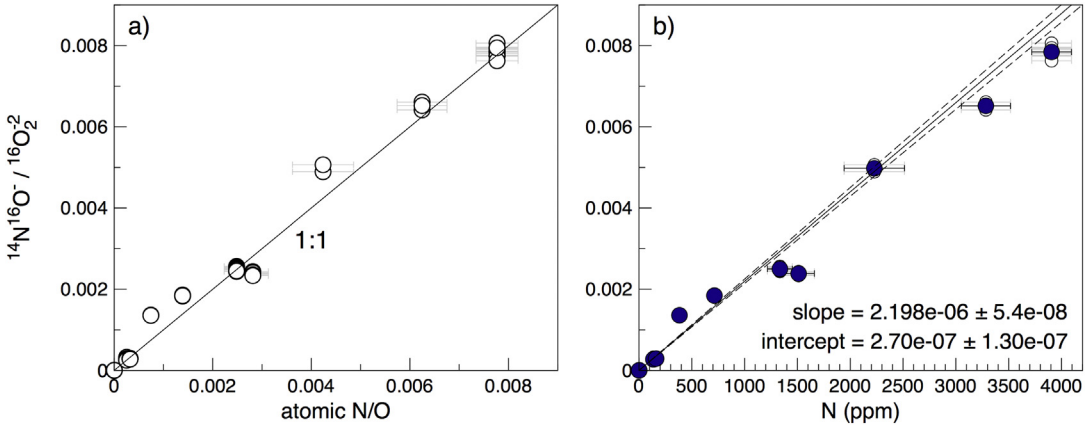

Fig. 4. Relationship between the secondary ion intensity ratio $^{14}N^{16}O^-/^{16}O_2^-$ and a) the atomic N/O ratio, and b) the known nitrogen content of the glasses. Data are shown for the twelve glasses with nitrogen concentrations ≤3906 ppm (open symbols: individual analyses (n = 80); filled symbols: average for each calibrant). The data were regressed using IsoplotR (Vermeesch, 2018).

related to the speciation of nitrogen, i.e., the water-rich glasses synthesized at high pressure likely contain a higher proportion of N-H species compared to N_2 than the "dry" glasses synthesized at atmospheric pressure (Dalou et al., 2017). Although the nitrogen speciation may affect the efficiency of ionization and N-O recombination reactions, individual analyses define a linear array with relatively low scatter (R^2 = 0.99, mean square weighted deviation (MSWD) = 1.7).

For isotope ratio measurements, the $^{14}N^{16}O^-$ and $^{15}N^{16}O^-$ ion intensities were initially measured for 6 and 25 s, respectively, for 60 cycles (Supplementary Table S3). Fig. 5 illustrates that for $^{14}N^{16}O^-$ count rates of ~4000 cps, the analytical precision of the $^{15}N/^{14}N$ isotope ratio is on the order of 5.6‰. Thus, the standard error of the mean (1σ) of each measurement is comparable to that predicted from Poisson statistics, and is controlled by the total number of counts of the less abundant $^{15}N^{16}O^-$ ion. The external reproducibility is judged from repeat analyses of the glass CB-2#3A (containing 162 ± 8 ppm N), which has a $\delta^{15}N$ value of −4 ± 1‰ (Humbert, 1998). For 10 measurements, average $^{15}N^{16}O^-/^{14}N^{16}O^-$ ratios of $3.737 \pm 0.039 \times 10^{-3}$ ($\delta^{15}N$ = 16.7 ± 10.5‰, 2σSD) and $3.749 \pm 0.063 \times 10^{-3}$ ($\delta^{15}N$ = 20.0 ± 17.1‰, 2σSD) are obtained (Supplementary Table S2) for 60 and 25 measurement cycles, respectively. These observations demonstrate that $^{15}N/^{14}N$ isotope ratios can be determined in the form of NO^- by SIMS with an analytical precision and reproducibility that is sufficient to resolve inter- and intra-sample nitrogen isotope variations in extraterrestrial materials, provided they record a wide range of $\delta^{15}N$ values, i.e., between solar-like signatures ($\delta^{15}N$ = −383 ± 8‰; Marty et al., 2011) and ^{15}N-hotspots (4200 ± 1500‰ to 4900 ± 300‰; Bonal et al., 2010; Briani et al., 2009).

3.3. Nitrogen analysis in the form of AlN^- and SiN^- at masses 41 to 45

By closing the entrance (18 µm) and exit slits (53 µm), the mass resolution was increased to 18,000 while still maintaining good transmission and flat-topped peaks. This setting allows the AlN^- and SiN^- molecular ions to be targeted for nitrogen measurements through the mass sequence $^{27}Al^{14}N^-$ (6 s), $^{28}Si^{14}N^-$ (6 s), $^{27}Al^{16}O^-$ (3 s), $^{28}Si^{16}O^-$ (3 s), $^{30}Si^{14}N^-$ (6 s), and $^{30}Si^{15}N^-$ (20s) for 20 cycles (Supplementary Table S4). However, resolving all possible interferences from the peaks of interest is challenging or, in some cases, impossible.

The high-resolution mass spectrum at mass 41 (Fig. 6), obtained with a MRP of 18,000, shows that nitrogen concentrations can be determined in the form of $^{27}Al^{14}N^-$, with an ion yield that is comparable to that of $^{12}C^{14}N^-$ or $^{14}N^{16}O^-$ for the glasses analyzed here (i.e., ~1.5 cps/ppmN/nA). A good second order polynomial correlation (R^2 = 0.98) is observed between the secondary ion intensity ratio $^{27}Al^{14}N^-/^{27}Al^{16}O^-$ and the known nitrogen content of the glasses, normalized by the Al_2O_3 content (Fig. 7a). The non-linearity is controlled by the nitrogen-richest glasses 710 and 711, and may possibly be related to the nitrogen speciation. It should be noted that with a MRP of 18,000, interferences from $^{30}Si^{11}B$ and $^{28}Si^{12}CH$ with the $^{27}Al^{14}N^-$ peak cannot be resolved; contributions from these masses are expected to significantly affect the $^{27}Al^{14}N^-$ signal for N-poor glasses. Thus, the nitrogen-poorest calibrant CM-1#13 (0.022 ± 0.034 ppm N) yields an apparent $^{27}Al^{14}N^-$ signal of ~700 cps (Supplementary Table S4). A mass resolution of 24,400 would be needed to separate $^{30}Si^{11}B$ from $^{27}Al^{14}N^-$, whereas $^{28}Si^{12}CH$ cannot be resolved from the $^{27}Al^{14}N^-$ peak. Furthermore, isotope ratio analyses ($^{27}Al^{15}N^-/^{27}Al^{14}N^-$) would

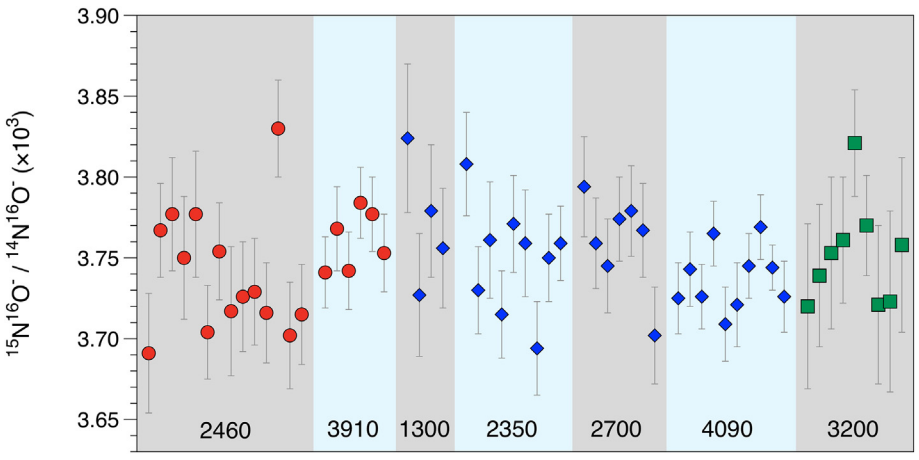

Fig. 5. Measured $^{15}N^{16}O^-/^{14}N^{16}O^-$ ratios for glass CB-2#3A (containing 162 ± 8 ppm N) determined with a mass resolution of 11,000 (red circles), 12,000 (blue diamonds), and 14,000 (green squares). The true $^{15}N/^{14}N$ ratio is ~0.003661. The variable $^{14}N^{16}O^-$ count rates of 1300 to 4090 cps indicated at the bottom were obtained by changing the width of the entrance and exit slits, as well as the width of the field aperture, and the primary ion beam current (Supplementary Table S3). Error bars represent the analytical precision (1σ) of individual analyses. (For interpretation of the references to colour in this figure legend, the reader is referred to the web version of this article.)

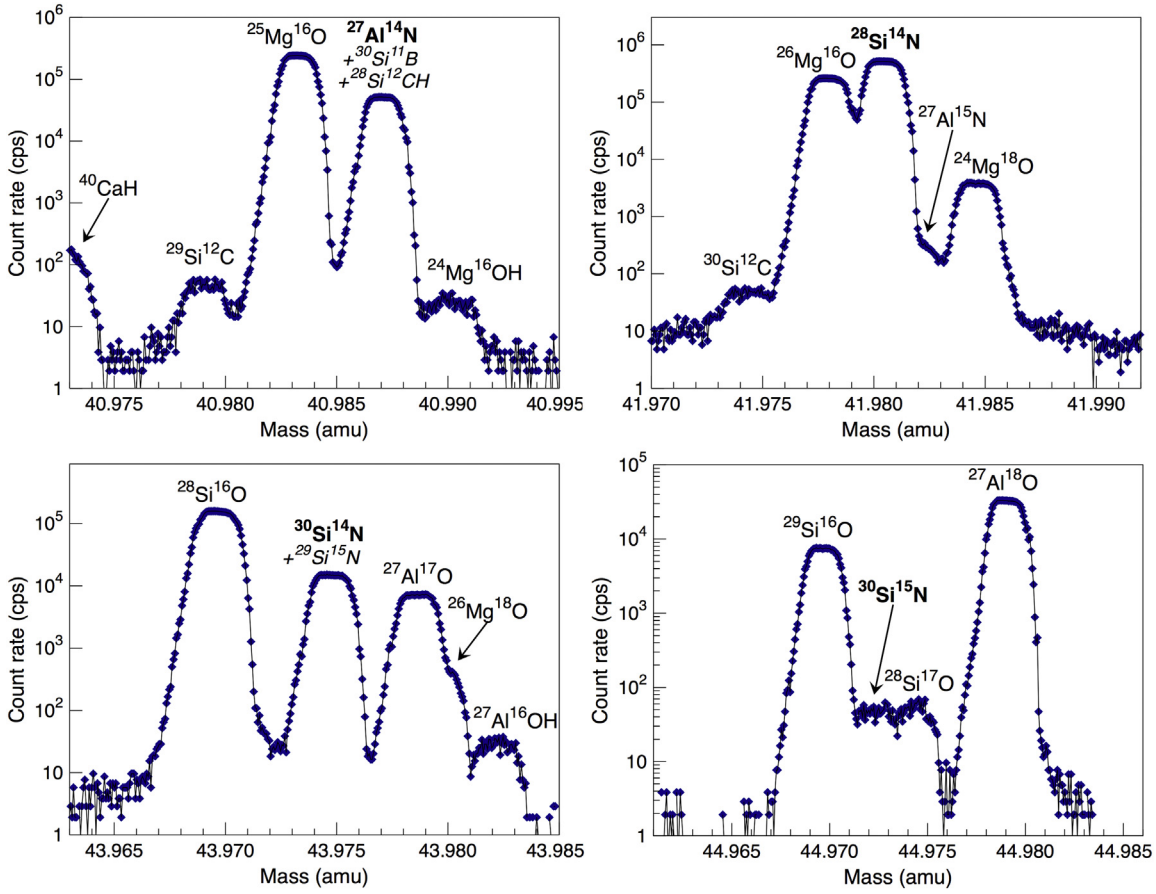

Fig. 6. High-resolution mass spectra at mass stations 41, 42, 44, and 45 for glass CB-2#1 (containing 3906 ± 188 ppm N) obtained with a mass resolution (m/Δm) of 18,000.

require a MRP of 25,440 in order to completely separate the $^{27}Al^{15}N^-$ peak from $^{28}Si^{14}N^-$.

Secondary SiN^- ions can be targeted for nitrogen abundance analyses at masses 42 ($^{28}Si^{14}N^-$), 43 ($^{29}Si^{14}N^-$; *not shown*), and 44 ($^{30}Si^{14}N^-$). Although the $^{27}Al^{15}N^-$ peak is not completely separated from $^{28}Si^{14}N^-$ at the given mass resolution, its contribution to the measured signal is negligible. Importantly, the yield of $^{28}Si^{14}N^-$ is on the order of 15 cps/ppmN/nA for all (C-)N-bearing synthetic basaltic glasses analyzed here. This yield is significantly greater than that of all other species targeted in this study, indicating that $^{28}Si^{14}N^-$ is the secondary molecular ion of choice for determining nitrogen concentrations in silicate glasses. An excellent correlation ($R^2 = 0.99$) is obtained between the secondary ion intensity ratio $^{28}Si^{14}N^-/^{28}Si^{16}O^-$ and the known nitrogen concentrations, normalized by the SiO_2 content (Fig. 7b). In this case, the non-linearity of the calibration curve is controlled by all samples with nitrogen contents ≥3906 ppm. Isotope ratio measurements are not feasible by this approach because the $^{28}Si^{15}N^-$ peak cannot be separated from $^{27}Al^{16}O^-$ (*not shown*; a mass resolution of > 72,800 would be required), and the $^{29}Si^{15}N^-$ peak virtually coincides with that of $^{30}Si^{14}N^-$.

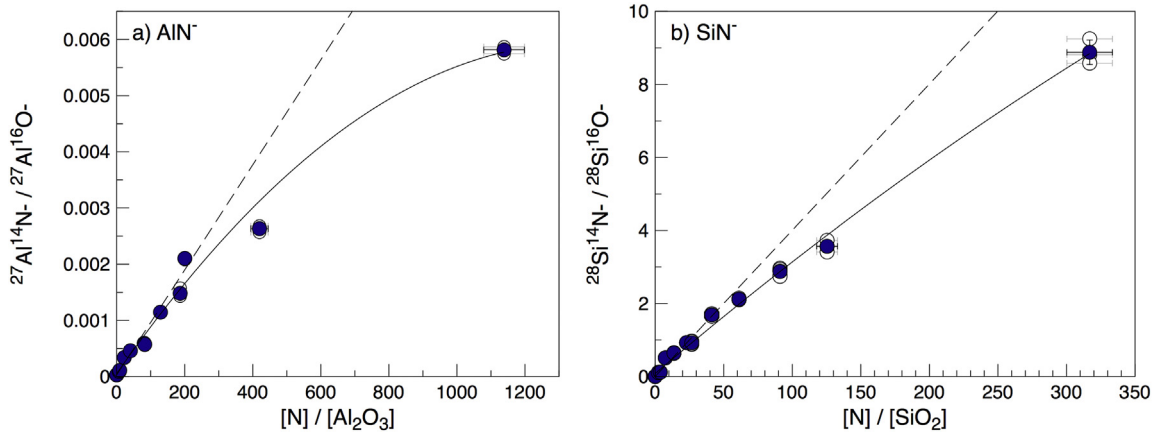

Fig. 7. Relationship between the secondary ion intensity ratios a) $^{27}Al^{14}N^-/^{27}Al^{16}O^-$ and b) $^{28}Si^{14}N^-/^{28}Si^{16}O^-$ and the known nitrogen content of the basaltic glasses, normalized by the Al_2O_3 and SiO_2 content, respectively. Calibration curves are shown as solid lines in the form of second order polynomial regressions (open symbols: individual analyses; filled symbols: average for each calibrant). Linear regression lines are indicated by the dashed lines.

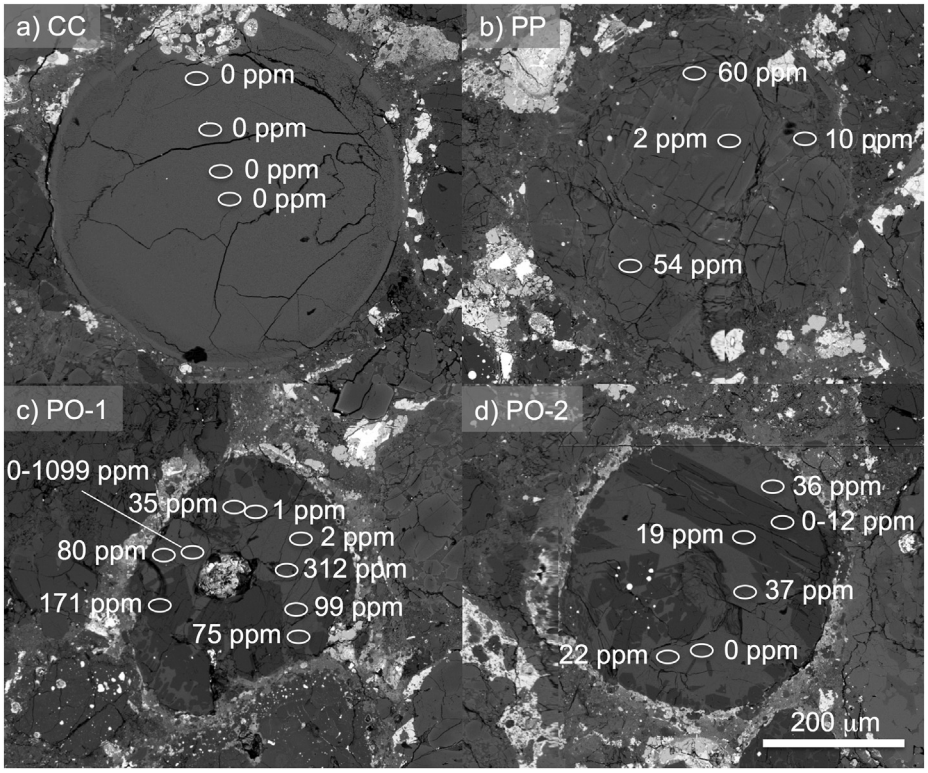

Fig. 8. Backscattered electron images of a cryptocrystalline (a), porphyritic pyroxene (b), and two porphyritic olivine (c, d) chondrules of the ordinary chondrite Semarkona. SIMS spots are labeled with the measured nitrogen concentrations. $^{15}N/^{14}N$ ratios for spot analyses with $N > 30$ ppm are reported in Table 2.

Table 2
Nitrogen content and isotopic composition, as well as measured ^{27}Al count rates (normalized to the primary beam intensity, I_p), of olivine, pyroxene, and mesostasis in four Semarkona chondrules.

Sample ID	N (ppm)	$\delta^{15}N$ (‰)	$^{27}Al/I_p$ (cps/nA)
CC-1	0	–	10,593
CC-2	0	–	10,334
CC-3	0	–	10,405
CC-4	0	–	10,153
PP-pyroxene	54 ± 11	−36 ± 50	471
PP-pyroxene	2 ± 2	–	364
PP-mesostasis	10 ± 3	–	46,381
PP-mesostasis	60 ± 9	−27 ± 44	26,382
PO-1-olivine	171 ± 26	21 ± 46	4717
PO-1-mesostasis	2 ± 2	–	249,345
PO-1-mesostasis	75 ± 23	−25 ± 98	256,883
PO-1-mesostasis	99 ± 16	−5 ± 46	231,436
PO-1-mesostasis	312 ± 27	0 ± 35	226,164
PO-1-mesostasis	80 ± 18	−12 ± 49	258,516
PO-1-mesostasis	0	–	252,227
	1099 ± 168	3 ± 89	247,150
PO-1-mesostasis	1 ± 1	–	225,728
PO-1-mesostasis	35 ± 6	28 ± 63	245,171
PO-2-olivine	0	–	7615
	12 ± 3	–	8089
PO-2-olivine	19 ± 5	–	5613
PO-2-mesostasis	36 ± 7	−29 ± 61	258,623
PO-2-mesostasis	37 ± 8	55 ± 72	266,287
PO-2-mesostasis	0	–	251,185
PO-2-mesostasis	22 ± 7	–	230,590
CM-1#4A			184,577
CM-1#3H			323,489

4. Nitrogen analysis of Semarkona chondrules

Individual bulk chondrules of ordinary chondrites record a wide range of nitrogen concentrations (0.8 to 61 ppm) and isotope compositions ($\delta^{15}N \approx -100$ to $+170$‰), which have been attributed to chondrule precursors with distinct nitrogen signatures (Das and Murty, 2009; Fredriksson et al., 1985; Mahajan and Murty, 2003; Murty and Marti, 1985). In order to investigate, for the first time, the intra-chondrule nitrogen distribution using SIMS, we targeted four chondrules of Semarkona (LL3.0) – the most primitive, least metamorphosed of all known ordinary chondrites (Alexander et al., 2012). The selected chondrules show distinct textures: cryptocrystalline (CC; Fig. 8a), porphyritic pyroxene (PP; Fig. 8b), and porphyritic olivine (PO; Fig. 8c,d).

The analytical approach used for the chondrules was nearly identical to the one described in Section 3.2, i.e., nitrogen was analyzed in the form of NO^-, together with $^{30}Si^-$ and $^{16}O_2^-$ in peak-jumping mono-collection mode. In addition, the $^{27}Al^-$ signal was monitored in order to distinguish the chondrule mesostasis from olivine and pyroxene. A mass resolution of 14,000 was chosen to improve the separation of the $^{15}N^{16}O^-$ peak from $^{29}SiH_2^-$. In this case, the analytical precision (1σ) of individual $^{15}N^{16}O^-/^{14}N^{16}O^-$ ratio analyses of the glass CB-2#3A (containing 162 ± 8 ppm N) is on the order of 12‰ (Fig. 5). The nitrogen content of the chondrule phases was derived from the relationship between the secondary ion intensity ratio $^{14}N^{16}O^-/^{16}O_2^-$ and the known nitrogen content of the reference materials shown in Fig. 4b. This calibration is not really appropriate for determining the nitrogen content of silicate minerals because possible matrix effects are not accounted for; in contrast, it can be used for the mesostasis in Semarkona chondrules which has a major element composition similar to that of the reference glasses (SiO_2 = 45.3 to 63.7 wt % and Al_2O_3 = 14.6 to 26.8 wt%; Grossman et al., 2002).

Nitrogen concentrations and isotopic compositions of the selected Semarkona chondrules are given in Table 2. The $\delta^{15}N$ values are reported for measurement spots with > 30 ppm nitrogen. Measured ^{27}Al count rates (normalized to the primary beam intensity of ~10 nA) are also reported in Table 2, together with the average values of the glasses CM-1#4A (16.50 wt% Al_2O_3) and CM-1#3H (22.38 wt% Al_2O_3) for comparison. Based on the calibrant analyses, the PO chondrule

mesostasis is estimated to contain ~18 to 20 wt% Al_2O_3, consistent with the range of Al_2O_3 values (i.e., 14.6 to 26.8 wt%) reported by Grossman et al. (2002) for mesostasis in Semarkona chondrules.

The results reveal that the cryptocrystalline chondrule does not contain any detectable nitrogen, whereas the porphyritic chondrules show a significant range of nitrogen concentrations between ≤10 to 312 ± 27 ppm (Fig. 8, Table 2). The highest abundances are detected in the mesostasis, but even some spot analyses of olivine and pyroxene yield a significant $^{14}N^{16}O^-$ signal, corresponding to several 10s of ppm nitrogen. While Li et al. (2015) showed that terrestrial olivine and pyroxene can contain such amounts of nitrogen at upper mantle conditions due to ion substitutions or interstitial impurities, the presence of N-rich mineral or glass inclusions in chondrule silicate phases cannot be ruled out (Varela et al., 2003). Strikingly, during one analysis of the PO-1 chondrule mesostasis, the nitrogen content abruptly increased from 0 ppm near the surface to 1099 ± 168 ppm after 20 measurement cycles. Based on the composition of nebular gas, i.e., $P_{H2} = 10^{-3}$ atm and $N_2/H_2 \approx 1 \times 10^{-4}$ (Anders and Grevesse, 1989), and the redox conditions during the formation of Semarkona chondrules, i.e., logfO_2 = IW −4 to +1 (Villeneuve et al., 2015), < 1 ppm nebular nitrogen can be physically or chemically dissolved into a basaltic melt (i.e., the only conditions for which the N solubility as a function of fO_2 has been determined; Libourel et al., 2003). The nitrogen concentrations observed in the Semarkona chondrule mesostasis are significantly higher than that, thus requiring increased nitrogen partial pressures compared to canonical conditions during chondrule formation – a scenario that has been invoked for other volatile elements trapped in chondrules (Marrocchi et al., 2016, and references therein) – or, alternatively, incorporation of nitrogen-rich precursors (Das and Murty, 2009). Although the nature of the nitrogen host phase cannot be identified here, the results demonstrate that the nitrogen distribution within olivine, pyroxene, and mesostasis in Semarkona chondrules is highly heterogeneous at the micron scale.

The $\delta^{15}N$ values vary between −36 ± 50 ‰ and + 55 ± 72‰. Although the uncertainties, reported at the 2σ level, are large compared to those obtained by static mass spectrometry analyses, the data fall within the range of values previously obtained for bulk chondrules of ordinary chondrites. It should be noted that all chondritic meteorite samples contain cosmogenic ^{15}N produced in the lattice of silicates during space exposure (Mathew and Murty, 1993); however, spallation reactions have a negligible effect on the nitrogen isotope signature for the concentrations observed here (see Füri et al., 2015b, for details), provided that the chondrules did not experience any significant pre-exposure to solar cosmic rays prior to accretion (Riebe et al., 2017, and references therein). Thus, the new data reveal that silicates (olivine, pyroxene, and mesostasis) are not the host phases of particularly ^{15}N-poor nitrogen in Semarkona chondrules, and they carry a nitrogen component that is clearly distinct from solar ($\delta^{15}N_{solar} = -383 \pm 8$‰; Marty et al., 2011). These observations are consistent with the notion, derived from the nitrogen analysis of a calcium-aluminum-rich inclusion in the CV3 chondrite NWA 8616, that the inner regions of the protoplanetary disk were contaminated with ^{15}N-rich material early in Solar System history (Füri et al., 2015b).

5. Conclusions and outlook

The lack of suitable N-bearing standards, as well as of a high-mass-resolution analytical protocol, has so far prevented the use of SIMS for nitrogen isotope analyses of silicate glasses. For this study, we have developed a suite of twelve (C-)N-rich synthetic basaltic glasses, containing between < 1 and 18,443 ± 966 ppm N, that can serve as reference materials for nitrogen analyses in the form of the CN^-, NO^-, AlN^-, and SiN^- (and MgN^-). Given the high mass resolution that can be achieved with the CAMECA IMS 1280 HR2, significant isobaric interferences from neighboring masses on these secondary molecular ions can be resolved. The high ion yield of $^{28}Si^{14}N^-$ makes it the ion of choice for determining nitrogen concentrations; however, isotope ratios can only be determined in the form of $^{12}C^{15}N^-/^{12}C^{14}N^-$ and $^{15}N^{16}O^-/^{14}N^{16}O^-$. Hence, the nitrogen signature of natural silicate samples, which may contain a very low and/or variable amount of carbon, is best investigated by targeting NO^- with a MRP of ≥10,725.

While the N-rich basaltic glass calibrants developed and characterized in our laboratory allow the intensity of secondary molecular nitrogen ions to be related to the nitrogen concentration, possible matrix effects on the ion yields remain to be evaluated by studying silicate glasses of variable chemical compositions (e.g., rhyolitic glasses). In addition, the effect of the nitrogen speciation (N_2 vs. N-H species) on the efficiency of ionization and recombination reactions will have to be investigated because, depending on the redox conditions, a range of nitrogen species may be present in natural silicate samples.

The analytical protocol developed here permits, for the first time, to study the concentration and isotopic composition of nitrogen trapped within micron-sized silicate phases such as chondrule mesostasis. It can also be applied for the analysis of melt inclusions in both terrestrial and extraterrestrial samples, and, thus, it may be key for improving our understanding of the nitrogen characteristics of the deep Earth and other planetary interiors.

Acknowledgements

We gratefully acknowledge L. Zimmermann, J. Villeneuve, and N. Boudin for assistance and support during the nitrogen analyses by static mass spectrometry and SIMS. We also thank L. Tissandier and L. Piani for fruitful discussions. Two anonymous reviewers are thanked for constructive comments, which helped improve the manuscript, as is Dr. Klaus Mezger for editorial handling. This work was supported by the European Research Council (grant no. 715028). This is CRPG-CNRS contribution 2592.

Appendix A. Nitrogen analysis by CO_2 laser extraction static mass spectrometry

Nitrogen abundances and isotope ratios of the glasses were determined by CO_2 laser extraction static mass spectrometry at the CRPG noble gas analytical facility (see Hashizume and Marty, 2004 and Humbert et al., 2000 for details). For the N-bearing basaltic glasses synthesized at atmospheric pressure, results are reported in Humbert (1998). Data for the C-N-bearing basaltic glasses synthesized at high pressure are given in Table A1. For each experimental run product, 2 to 3 replicate analyses were carried out on fragments between 37 and 436 μg in mass. Several samples were reheated after melting to ensure that the total amount of nitrogen was extracted during the first heating step. Isotope ratios of nitrogen ($^{15}N/^{14}N$) are expressed in the delta (δ) notation, where $\delta^{15}N = [(^{15}N/^{14}N)_{sample} / (^{15}N/^{14}N)_{std} - 1] \times 1000$, in ‰, and the standard is atmospheric nitrogen with $^{15}N/^{14}N = 0.003676$. Given the high nitrogen content of the glasses, blank contributions (9.58×10^{-13} mol N) were negligible (< 0.1%). The reproducibility of air standard abundance and isotope ratio measurements was ± 1.1% and ± 2.5‰ (1σ), respectively.

Table A1
Nitrogen abundance and isotopic composition of the six C-N-bearing basaltic glasses synthesized at high pressure.

Sample	Heating step	Mass (μg)	N (ppm)	
704	1	176	407 ± 4	−3.1 ± 2.5
	2		2	−0.3 ± 22.0
704	1	212	360 ± 4	−0.7 ± 2.5
703	1	95	776 ± 8	−5.4 ± 3.2
703	1	182	648 ± 7	−3.0 ± 2.5
	2		3	23.2 ± 10.1
703	1	51	720 ± 8	−9.9 ± 2.5
702	1	98	2025 ± 22	−7.7 ± 2.6
702	1	436	2430 ± 26	−9.5 ± 2.5
701	1	256	3449 ± 37	−8.9 ± 2.5
701	1	37	3120 ± 33	−7.3 ± 3.0
710	1	158	6505 ± 69	−9.0 ± 2.5
	2		32	−17.2 ± 7.8
710	1	145	7334 ± 78	−9.7 ± 2.5
710	1	292	6812 ± 73	−3.9 ± 3.0
	2		40	−8.6 ± 2.6
711	1	65	18,782 ± 200	−6.3 ± 2.5
711	1	225	19,193 ± 205	−6.6 ± 2.5
711	1	245	17,353 ± 185	−8.6 ± 2.6
	2		39	−10.0 ± 6.1

Appendix B. Water and carbon analysis by SIMS

The water and carbon content of the glasses was determined using the CAMECA 1280 HR2 ion microprobe at the CRPG. A ~6 nA primary ion beam of Cs^+ was focused on a ~20 μm diameter area, and a normal-incidence electron gun was used for charge compensation. Negative secondary ions ^{12}C, ^{16}O, ^{17}O, $^{16}O^1H$, ^{27}Al, and ^{28}Si were measured in peak jumping mode with a mass resolution of 8000. The ^{12}C signal was determined by ion counting on an EM, whereas all other ions were measured on a Faraday cup. A 20 μm × 20 μm raster was used for 120 s prior to analysis to remove any surface contamination. Each analysis consisted of 10 cycles, with a counting time of 3 s on each peak.

A suite of seven in-house (basaltic) SIMS standards with known H_2O and CO_2 concentrations was used for calibration, and concentrations of H_2O and CO_2 in the N-bearing basaltic glasses were calculated using best-fit regressions for $^{16}O^1H/^{16}O$ versus H_2O and $^{12}C/^{16}O$ versus CO_2, respectively. The water content of all basaltic glasses synthesized at atmospheric pressure is below the detection limit, and only sample CB-2#1 contains a detectable amount of carbon (122 ± 21 ppm CO_2) (Table 1). In contrast, the water concentrations of the glasses synthesized at high pressure vary between 0.8 and 2.4 wt% (Table 1). Samples 702 (391 ± 26 ppm CO_2), 704 (241 ± 21 ppm CO_2), and 710 (565 ± 45 ppm CO_2) appear to contain a relatively homogeneous concentration of carbon, although only three spots were analyzed on each grain. The other three samples (701, 703, 711) yielded extremely variable $^{12}C^-$ signals at different spots on the same grain. For example, the CO_2-equivalent carbon content varies between 916 and 15,400 ppm in sample 711, and between 105 and 31,500 ppm in sample 703. This heterogeneity is inferred to be due to the presence of small (≤3 μm) graphite inclusions, clustered in some parts of the glasses, as observed by scanning electron microscope imaging.

'Water' concentrations are reported as total H_2O (Table 1). However, depending on the experimental conditions, the glasses likely contain various hydrous species, including OH, H_2, as well as N-H or C-H compounds (Armstrong et al., 2015; Dalou et al., 2016, 2017). Therefore, the reported 'water' abundances may represent contributions from all of these species as a result of dissociation of molecular ions and recombination reactions that occur at or near the sample surface during sputtering. Similarly, 'carbon' abundances are reported as total CO_2 but may, in fact, represent a range of C-H and/or C-O species (Armstrong et al., 2015).

Appendix C. Supplementary data

Supplementary data to this article can be found online at https://doi.org/10.1016/j.chemgeo.2018.06.008.

References

Aléon, J., Robert, F., Chaussidon, M., Marty, B., 2003. Nitrogen isotopic composition of macromolecular organic matter in interplanetary dust particles. Geochim. Cosmochim. Acta 67, 3773–3783. http://dx.doi.org/10.1016/S0016-7037(00)00170-4.

Alexander, C.M.O., Bowden, R., Fogel, M.L., Howard, K.T., Herd, C.D.K., Nittler, L.R., 2012. The provenances of asteroids, and their contributions to the volatile inventories of the terrestrial planets. Science 337, 721–723. http://dx.doi.org/10.1126/science.1223474.

Anders, E., Grevesse, N., 1989. Abundances of the elements: meteoritic and solar. Geochim. Cosmochim. Acta 53, 197–214.

Armstrong, L.S., Hirschmann, M.M., Stanley, B.D., Falksen, E.G., Jacobsen, S.D., 2015. Speciation and solubility of reduced C-O-H-N volatiles in mafic melt: implications for volcanism, atmospheric evolution, and deep volatile cycles in the terrestrial planets. Geochim. Cosmochim. Acta 171, 283–302. http://dx.doi.org/10.1016/j.gca.2015.07.007.

Bonal, L., Huss, G.R., Krot, A.N., Nagashima, K., Ishii, H.A., Bradley, J.P., 2010. Highly ^{15}N-enriched chondritic clasts in the CB/CH-like meteorite Isheyevo. Geochim. Cosmochim. Acta 74, 6590–6609. http://dx.doi.org/10.1016/j.gca.2010.08.017.

Briani, G., Gounelle, M., Marrocchi, Y., Mostefaoui, S., Leroux, H., Quirico, E., Meibom, A., 2009. Pristine extraterrestrial material with unprecedented nitrogen isotopic variation. Proc. Natl. Acad. Sci. U. S. A. 106, 10522–10527. http://dx.doi.org/10.1073/pnas.0901546106.

Busemann, H., Young, A.F., Alexander, C.M.O.'.D., Hoppe, P., Mukhopadhyay, S., Nittler, L.R., 2006. Interstellar chemistry recorded in organic matter from primitive meteorites. Science 312, 727–730. http://dx.doi.org/10.1126/science.1123878.

Dalou, C., Hirschmann, M.M., von der Handt, A., Mosenfelder, J., Armstrong, L.S., 2016. Nitrogen and carbon fractionation during core-mantle differentiation at shallow

depth. Earth Planet. Sci. Lett. 458, 141–151. http://dx.doi.org/10.1016/j.epsl.2016.10.026.
Dalou, C., Le Losq, C., Hirschmann, M.M., Jacobsen, S., Füri, E., 2017. Evolution of C-O-H-N volatile species in the magma ocean during core formation. Eos. Trans. AGU Fall Meet. Abstr. V31E–01.
Das, J.P., Murty, S.V.S., 2009. Trapped nitrogen in individual chondrules: nature of chondrule precursors and clues to formation mechanisms. J. Geophys. Res. 114, 1–16. http://dx.doi.org/10.1029/2008JE003232.
Deloule, E., Robert, F., 1995. Interstellar water in meteorites? Geochim. Cosmochim. Acta 59, 4695–4706. http://dx.doi.org/10.1016/0016-7037(95)00313-4.
Fredriksson, K., Murty, S.V.S., Marti, K., 1985. Some chemical and isotopic observations in chondrules. Meteoritics 20, 347–357.
Frick, U., Pepin, R.O., 1981. Microanalysis of nitrogen isotope abundances: association of nitrogen with noble gas carriers in Allende. Earth Planet. Sci. Lett. 56, 64–81.
Füri, E., Marty, B., 2015. Nitrogen isotope variations in the Solar System. Nat. Geosci. 8, 515–522. http://dx.doi.org/10.1038/ngeo2451.
Füri, E., Barry, P.H., Taylor, L.A., Marty, B., 2015a. Indigenous nitrogen in the Moon: constraints from coupled nitrogen–noble gas analyses of mare basalts. Earth Planet. Sci. Lett. 431, 195–205. http://dx.doi.org/10.1016/j.epsl.2015.09.022.
Füri, E., Chaussidon, M., Marty, B., 2015b. Evidence for an early nitrogen isotopic evolution in the solar nebula from volatile analyses of a CAI from the CV3 chondrite NWA 8616. Geochim. Cosmochim. Acta 153, 183–201. http://dx.doi.org/10.1016/j.gca.2015.01.004.
Grossman, J.N., Alexander, C.M.O., Wang, J., Brearley, A.J., 2002. Zoned chondrules in Semarkona: evidence for high- and low-temperature processing. Meteorit. Planet. Sci. 37, 49–73.
Hashizume, K., Marty, B., 2004. Nitrogen isotopic analyses at the sub-picomole level using an ultra-low blank laser extraction technique. In: de Groot, P.A. (Ed.), Handbook of Stable Isotope Analytical Techniques. Elsevier Science, pp. 361–375.
Hauri, E.H., Wang, J., Pearson, D.G., Bulanova, G.P., 2002. Microanalysis of $\delta^{13}C$, $\delta^{15}N$, and N abundances in diamonds by secondary ion mass spectrometry. Chem. Geol. 185, 149–163.
Humbert, F., 1998. Solubilité de l'azote dans les silicates liquides. Université Henri Poincaré, Nancy.
Humbert, F., Libourel, G., France-Lanord, C., Zimmermann, L., Marty, B., 2000. CO_2-laser extraction-static mass spectrometry analysis of ultra-low concentrations of nitrogen in silicates. Geostand. Newslett. 24, 255–260.
Javoy, M., Pineau, F., 1991. The volatiles record of a "popping" rock from the Mid-Atlantic Ridge at 14°N: chemical and isotopic composition of gas trapped in the vesicles. Earth Planet. Sci. Lett. 107, 598–611. http://dx.doi.org/10.1016/0012-821X(91)90104-P.
Kadik, A.A., Kurovskaya, N.A., Ignat, Y.A., Kononkova, N.N., 2011. Influence of oxygen fugacity on the solubility of nitrogen, carbon, and hydrogen in FeO-Na_2O-SiO_2-Al_2O_3 melts in equilibrium with metallic iron at 1.5 GPa and 1400 °C. Geochem. Int. 49, 429–438. http://dx.doi.org/10.1134/S001670291105003X.
Kadik, A.A., Koltashev, V.V., Kryukova, E.B., VG, P., Tsekhonya, T.I., Kononkova, N.N., 2015. Solubility of nitrogen, carbon, and hydrogen in FeO-Na_2O-Al_2O_3-SiO_2 melt and liquid iron alloy: influence of oxygen fugacity. Geochem. Int. 53, 849–868. http://dx.doi.org/10.1134/S001670291510002X.
Kerridge, J.F., 1985. Carbon, hydrogen and nitrogen in carbonaceous chondrites: abundances and isotopic compositions in bulk samples. Geochim. Cosmochim. Acta 49, 1707–1714.
Kung, C.C., Clayton, R.N., 1978. Nitrogen abundances and isotopic compositions in stony meteorites. Earth Planet. Sci. Lett. 38, 421–435.
Lhuissier, F., Lefebvre, F., Gibouin, D., Demarty, M., Thellier, M., Ripoll, C., 2000. Secondary ion mass spectrometry imaging of the fixation of ^{15}N-labelled NO in pollen grains. J. Microsc. 198, 108–115.
Li, Y., Wiedenbeck, M., Shcheka, S., Keppler, H., 2013. Nitrogen solubility in upper mantle minerals. Earth Planet. Sci. Lett. 377–378, 311–323. http://dx.doi.org/10.1016/j.epsl.2013.07.013.
Li, Y., Huang, R., Wiedenbeck, M., Keppler, H., 2015. Nitrogen distribution between aqueous fluids and silicate melts. Earth Planet. Sci. Lett. 411, 218–228. http://dx.doi.org/10.1016/j.epsl.2014.11.050.
Libourel, G., Marty, B., Humbert, F., 2003. Nitrogen solubility in basaltic melt. Part I. Effect of oxygen fugacity. Geochim. Cosmochim. Acta 67, 4123–4135. http://dx.doi.org/10.1016/S0016-7037(03)00259-X.
Mahajan, R.R., Murty, S.V.S., 2003. Laser microprobe for the study of noble gases and nitrogen in single grains: a case study of individual chondrules from the Dhajala meteorite. Proc. Indian Natl. Sci. Acad. 112, 113–127. http://dx.doi.org/10.1007/BF02710047.
Marrocchi, Y., Chaussidon, M., Piani, L., Libourel, G., 2016. Early scattering of the protoplanetary disk recorded in meteoritic chondrules. Sci. Adv. 2, e1601001. http://dx.doi.org/10.1126/sciadv.1601001.
Marrocchi, Y., Villeneuve, J., Batanova, V., Piani, L., Jacquet, E., 2018. Oxygen isotopic diversity of chondrule precursors and the nebular origin of chondrules. Earth Planet. Sci. Lett. 496, 132–141. http://dx.doi.org/10.1016/j/epsl.2018.05.042.
Marty, B., Chaussidon, M., Wiens, R.C., Jurewicz, A.J.G., Burnett, D.S., 2011. A ^{15}N-poor isotopic composition for the solar system as shown by Genesis solar wind samples. Science 332, 1533–1536. http://dx.doi.org/10.1126/science.1204656.
Mathew, K.J., Marti, K., 2001. Early evolution of Martian volatiles: nitrogen and noble gas components in ALH84001 and Chassigny. J. Geophys. Res. 106, 1401–1422.
Mathew, K.J., Murty, S.V.S., 1993. Cosmic ray produced nitrogen in extra terrestrial matter. Proc. Indiana Acad. Sci. 102, 415–437.
Meibom, A., Krot, A.N., Robert, F., Mostefaoui, S., Russell, S.S., Petaev, M.I., Gounelle, M., 2007. Nitrogen and carbon isotopic composition of the Sun inferred from a high-temperature solar nebular condensate. Astrophys. J. 656, L33–L36. http://dx.doi.org/10.1086/512052.
Mosbah, M., Bastoul, A., Cuney, M., Pironon, J., 1993. Nuclear microprobe analysis of ^{14}N and its application to the study of ammonium-bearing minerals. Nucl. Instrum. Methods Phys. Res., Sect. A B77, 450–456.
Mostefaoui, S., Zinner, E., Hoppe, P., Stadermann, F.J., El Goresy, A., 2005. In situ survey of graphite in unequilibrated chondrites: morphologies, C, N, O, and H isotopic ratios. Meteorit. Planet. Sci. 743, 721–743.
Murty, S.V.S., Marti, K., 1985. Nitrogen isotopic abundance of individual chondrules. Lunar Planet. Sci. XVI, 605–606.
Pearson, V.K., Sephton, M.A., Franchi, I.A., Gibson, J.M., Gilmour, I., 2006. Carbon and nitrogen in carbonaceous chondrites: elemental abundances and stable isotopic compositions. Meteorit. Planet. Sci. 41, 1899–1918.
Presnall, D.C., Hoover, J.D., 1984. Composition and depth of origin of primary mid-ocean ridge basalts. Contrib. Mineral. Petrol. 87, 170–178.
Regier, M.E., Hervig, R.L., Myers, M.L., Roggensack, K., Wilson, C.J.N., 2016. Analyzing nitrogen in natural and synthetic silicate glasses by secondary ion mass spectrometry. Chem. Aust. 447, 27–39. http://dx.doi.org/10.1016/j.chemgeo.2016.10.019.
Riebe, M.E.I., Huber, L., Metzler, K., Busemann, H., Luginbuehl, S.M., Meier, M.M.M., Maden, C., Wieler, R., 2017. Geochim. Cosmochim. Acta 213, 618–634 doi:10/1016/j/gca/2017.06.035.
Roskosz, M., Bouhifd, M.A., Jephcoat, A.P., Marty, B., Mysen, B.O., 2013. Nitrogen solubility in molten metal and silicate at high pressure and temperature. Geochim. Cosmochim. Acta 121, 15–28. http://dx.doi.org/10.1016/j.gca.2013.07.007.
Sugiura, N., 1998. Ion probe measurements of carbon and nitrogen in iron meteorites. Meteorit. Planet. Sci. 33, 393–409.
Thiemens, M.H., Clayton, R.N., 1983. Nitrogen contents and isotopic ratios of clasts from enstatite chondrite Abee. Earth Planet. Sci. Lett. 62, 165–168.
Thomen, A., Robert, F., Remusat, L., 2014. Determination of the nitrogen abundance in organic materials by NanoSIMS quantitative imaging. J. Anal. At. Spectrom. 29, 512–519. http://dx.doi.org/10.1039/c3ja50313e.
Varela, M.E., Bonnin-Mosbah, M., Kurat, G., Gallien, J.-P., 2003. Nitrogen microanalysis of glass inclusions in chondritic olivines by nuclear reaction. Geochim. Cosmochim. Acta 67, 1247–1257. http://dx.doi.org/10.1016/S0016-7037(00)01204-8.
Vermeesch, P., 2018. IsoplotR: a free and open toolbox for geochronology. Geosci. Front. http://dx.doi.org/10.1016/j.gsf.2018.04.001. (in press).
Villeneuve, J., Libourel, G., Soulié, C., 2015. Relationship between type I and type II chondrules: implications on chondrule formation processes. Geochim. Cosmochim. Acta 160, 277–305 doi:10/1016/j.gca.2015.03.033.
von der Handt, A., Dalou, C., 2016. Quantitative EPMA of nitrogen in silicate glasses. Microsc. Microanal. 22, 1810–1811.
Zhang, Z., Hirschmann, M.M., 2016. Experimental constraints on mantle sulfide melting up to 8 GPa. Am. Mineral. 101, 181–192.
Zinner, E., Ming, T., Anders, E., 1989. Interstellar SiC in the Murchison and Murray meteorites: isotopic composition of Ne, Xe, Si, C, and N. Geochim. Cosmochim. Acta 53, 3273–3290.